Stijn Matthys is a Professor at Ghent University, where he received his PhD and MSc. He is also the Technology Development Manager at UGent DuraBUID Materials and Convenor of *fib* (International Federation for Structural Concrete) Task Group 9.3 on FRP Reinforcement for Concrete Structures. His research interests include advanced composite reinforcement for concrete structures, behavior and design of structural concrete, rehabilitation, and monitoring of structures.

Luc Taerwe, FACI, is the Director of the Magnel Laboratory for Concrete Research, Dean of the Faculty of Engineering, and a Full Professor of concrete structures at Ghent University. He graduated as a civil engineer from Ghent University (Ghent, Belgium) where he also received his PhD. He is a member or chairman of several international technical committees dealing with concrete or concrete related topics, including ACI Committee 440, Fiber Reinforced Polymer Reinforcement.

INTRODUCTION

Strengthening of reinforced concrete members by means of externally bonded reinforcement (EBR) is an efficient technique, nowadays often used in practice. Various studies on the structural behavior of concrete elements strengthened in flexure have been reported, mainly in relation to 4-point bending tests. Detailed studies on the serviceability behavior, however, have been less frequently reported in literature. Nevertheless, tension stiffening behavior and modeling for FRP strengthened concrete members at serviceability limit state has been reported by a number of authors.[1-8]

To study the behavior of steel reinforced concrete beams strengthened in flexure with externally bonded carbon FRP (CFRP) reinforcement, four-point bending tests were performed on nine large-scale beams with a rectangular cross-section (total depth 450 mm [17.7 in.], width 200 mm [7.9 in.]) and span length 3.8 m [150 in.], considering both prefabricated and wet lay-up CFRP types. Different amounts of internal and external reinforcement and different load histories were considered. The positive influence of the FRP EBR on the serviceability behavior has been observed in these flexural tests. To study the serviceability aspect further with respect to tension stiffening and cracking, further tests have been conducted on strengthened tensile members. Eighteen 'tension stiffening' tests were performed on concrete prisms with embedded steel reinforcing bar. The prisms have side length 100 mm [3.9 in.] and total length 1100 or 1200 mm [43.3 or 47.2 in.]. The parameters selected for these tests included type of FRP, concrete strength and amount of internal and external reinforcement.

Based on this experimental work, existing models for the tension stiffening, cracking behavior and deflections have been extended to include the influence of the externally bonded FRP reinforcement.

RESEARCH SIGNIFICANCE

For flexural members strengthened with FRP EBR, the serviceability behavior may often govern the design (especially if early debonding is avoided). This is due to the high strength of FRP materials. The cross-sectional area of bonded FRP reinforcement to fulfill ultimate limit state (ULS) conditions, may often be less than the cross-sectional area needed to fulfill the serviceability limit state (SLS). In any case, the serviceability behavior is a crucial aspect of design. Hence, proper prediction models for the SLS are important, yet have so far been less investigated than the ULS.

EXPERIMENTAL INVESTIGATION: FOUR-POINT BENDING

Outline of the experiments

The test specimens consisted of nine reinforced concrete (RC) beams with rectangular cross-section, two of which are reference specimens. The beams have a width of 200 mm [7.9 in.], a total depth of 450 mm [17.7 in.], a span of 3.8 m [150 in.] and a total length of 4.0 m [157 in.]. The dimensions of the beams and the test set-up are shown in Fig. 1. The test parameters are given in Table 1. A first series of beams (BF1 to BF6) is characterized by a steel reinforcement ratio $\rho_s = A_s/bd$ of 0.96 % and is strengthened (except for the reference beam BF1) with one layer of CFRP. These beams allow the investigation of the variability of the strengthening effect (BF2/BF3), the influence of pre-cracking (BF4) and load application prior to strengthening (BF5). The load level for pre-cracking and pre-loading (point loads Q equal to 110 kN [24.7 kips]), was taken equal to the service load of the unstrengthened beam (based on observed deflections). For beam BF6, an extra FRP-end anchorage was provided to verify if the FRP debonding failure, obtained for the tested beams, initiated at the FRP ends or by intermediate crack bridging.

In a second series of beams (BF7 to BF9), half the amount of longitudinal steel reinforcement of the first series was provided. Beam BF7 is the reference specimen, while beams BF8 and BF9 are strengthened in flexure by means of two different types of CFRP (prefabricated and wet lay-up CFRP).

For all beams the same concrete type was used, with a mean compressive cylinder strength f_{cm} at 28 days of 32.8 MPa [4757 psi]. For the internal reinforcement deformed steel bars were used, with a guaranteed characteristic yield stress of 500 MPa [72,520 psi] and a diameter of 16 mm [0.63 in.]. The externally bonded reinforcement consisted of 1 layer CFRP strip (type CarboDur, width 100 mm [3.9 in.], thickness 1.2 mm [0.047 in]), except for beam BF9 for which 2 layers wet lay-up CFRP sheet (Replark, width 100 mm [3.9 in.], nominal thickness of one layer 0.111 mm [0.0044 in.]) were used. The length of the FRP EBR was taken as 3.66 m [144 in.] (maximum practically possible between the supports). The extra U-shaped anchorage provided for BF6, consisted of 1 layer Replark (width 330 mm [13.0 in.]). The main characteristics of the reinforcement, obtained by tensile testing, are summarized in Table 2. The external CFRP reinforcement was applied to the beams according to the procedures specified by the suppliers. Preparation of the concrete surface included sand blasting for beams BF2 till BF5, while grinding was used for beams BF6, BF8 and BF9. Before strengthening, beam BF4 was loaded up to a point load of 110 kN [24.7 kips] and unloaded. For beam BF5, a point load of 110 kN [24.7 kips] was applied prior to strengthening and curing.

During the tests,[2] both manual and electronic measurements were taken, including midspan deflection, concrete, steel and FRP deformations in the central zone of the beam, strain distribution of the FRP along one half of the beam, appearance and development of cracks and crack widths.

Main test results

The strengthened beams failed by intermediate crack debonding after yielding of the internal reinforcement. Strengthening ratio's up to 38% were obtained, whereas for the tested beams no significant influence was observed on the failure load by pre-cracking the specimen. The beam strengthened under service load, failed at 95% of the ultimate load of the beams strengthened under self weight. For a further discussion on the test results at ultimate state, refer to Reference 2. In the following sections, the test results in terms of service behavior are discussed further.

Load-deflection behavior

A comparison of the load-deflection response of the beams is shown in Fig. 2 and 3. In these figures, the curve for beam BF3 is not shown as it almost exactly matches that of beam BF2. The recorded load-deflection curves clearly show the increase of the stiffness in the cracked state, proportional to the amount of FRP material. Also beam BF5, which is strengthened under full service load of the reference specimen, demonstrates a clear increase of flexural stiffness after strengthening (Fig. 2). A similar result is obtained for beam BF4, which was pre-cracked, unloaded and then strengthened (Fig. 3).

Further to the higher stiffness, a significant increase is obtained of the load at which the internal steel reinforcement starts yielding.

Cracking behavior

All beams started cracking at about the same load level $Q_{cr} \approx 18$ kN [4.0 kips]. The mean crack widths of beams BF1, BF2, BF4, BF7, BF8 and BF9 are compared in Fig 4. From this figure, the restraining effect of the CFRP strengthening on the crack width is noted. For beams BF4 (which was pre-cracked) and BF9 (with a very low FRP reinforcement ratio), this restraining effect is rather limited. The favorable influence of FRP EBR on the cracking behavior is in agreement with the increased stiffness in the cracked state of the strengthened beams.

EXPERIMENTAL INVESTIGATION: TENSION STIFFENING

Outline of the experiments

A total of 18 concrete prisms with side length of 100 mm [3.9 in.] and total length of 1200 mm [47.2 in.] (1100 mm [43.3 in.] for batch T1), 14 of which strengthened with FRP EBR, were subjected to axial tension according to the test set-up shown in Fig. 5. Reinforcement ratios of the internal and external reinforcement, FRP type and concrete grade were considered as parameters. An overview of the different specimens, their designation and the corresponding test parameters are given in Table 3. The internal reinforcement consisted of a centrally located deformed steel bar S500, with a characteristic yield strength of 500 MPa [72,520 psi] and a diameter of either 10, 14, or 16 mm [0.39, 0.55, or 0.63 in.]. The externally bonded reinforcement consisted of either CFRP sheets or GFRP fabrics. These were glued on two opposite faces of the concrete prism, impregnated and cured in-situ. For the CFRP, the Replark system (Replark Type 20 sheet/Epotherm Type XL 700 S epoxy) was used. The sheets have a width of 100 mm [3.9 in.] and the nominal thickness of one layer equals 0.111 mm [0.0044 in.]. For the GFRP fabrics, Roviglas G (Roviglas G fabric/Multipox epoxy) was used, with a width of 100 mm [3.9 in.] and a nominal one layer thickness of 0.100 mm [0.0039 in.]. The properties of the reinforcement are given in Table 2. For the concrete, both a normal-strength concrete (NSC) and a high-strength concrete (HSC) with a mean compressive cylinder strength at 28 days of, respectively, 32.8 and 96.0 MPa [4757 and 13,925 psi] were used.

Application of the external FRP reinforcement was executed 7 days before testing and included roughening of the concrete surface by means of grinding.

The prisms were tested in a deformation controlled way (movement of the actuator 0.1 mm/min [0.0039 in./min] in the initial phase and 1 mm/min [0.039 in./min] after the steel started yielding). The tensile force was applied by gripping of the steel reinforcement. To prevent steel yielding outside the concrete prism, three steel reinforcing bars were provided in the gripping zone. These were embedded in the concrete prisms over a distance of 100 mm [3.9 in.], whereas only one internal bar was provided in the central zone. To account for local stresses at the prism ends, also confinement hoop reinforcement was provided over a distance of 150 mm [5.9 in.] (Fig. 5). For specimens of batch T2 till T5, a mechanical anchorage was applied before testing. In this way the FRP bond failure at the prism ends, obtained for specimens T1, could be prevented. The anchorage device consists of tensile rods, transfer beams and steel plates glued on the FRP reinforcement as shown in Fig. 5. By pre-tensioning of the rods, a transverse compressive stress of about 3.5 MPa [508 psi] was applied on the ends of the external FRP reinforcement.

Concrete and FRP strains, crack development and crack widths were recorded during testing as a function of the applied load.

Main test results

Depending on the type and amount of externally bonded reinforcement and on the failure mode, strength increase between 1.3 and 3.0 was obtained. This is further discussed in Reference 2. In the following sections, the test results in terms of service behavior are discussed.

Mean tensile strain

The recorded tensile strains of some of the prisms are given in Figs. 6 and 7. In the latter figures, ε_m represents the mean value of the strain measurements, located on both the concrete and the FRP (for the strengthened prisms). For most of the prisms, the mean strain measured on the FRP covered side face and the mean strain of the free concrete surface were not significantly different. The load-strain behavior is compared based on an equivalent reinforcement ratio ρ_{eq}, defined as

$$\rho_{eq} = \rho_s + \frac{E_f}{E_s}\rho_f \tag{1}$$

with $\rho_r = A_r/A_c$ the reinforcement ratio (subscript s or f, for steel or FRP reinforcement, respectively), A_r and A_c the cross sectional area of the reinforcement and the concrete, and E_r the modulus of elasticity of the reinforcement. Values of ρ_s, ρ_f, and ρ_{eq} are given in Table 3.

Figure 6 compares strengthened prisms with the same amount of internal steel and with the same equivalent reinforcement ratio (about 1.83 %). The obtained curves are close to each other. A higher stiffness in the cracked state is obtained compared to the reference prism ($\rho_s = 1.56\%$). For the prism in HSC, the cracking load is higher.

In Fig. 7 the recorded deformations for strengthened prisms with increasing equivalent reinforcement ratio are shown. Higher stiffness in the cracked state is obtained with increasing equivalent reinforcement ratio. The slope of the last branch (stiffness in the cracked state after yielding of the steel) is almost the same for the three prisms with the same type and amount of external reinforcement, independent of the amount of internal steel reinforcement. Prior to yielding of the internal steel, this is not the case as these specimens with same type and amount of external reinforcement have an increasing amount of internal steel reinforcement.

Crack pattern

In Fig. 8 and 9, the crack pattern at ultimate load, the mean crack width and the crack spacing are compared for prisms N(T4)/100/16/Ref. and N(T4)/100/16/C#1. From these figures, it is observed that the crack pattern is influenced by both the internal steel and the external FRP reinforcement. A smaller crack spacing is obtained for an increasing amount of reinforcement, where already a small amount of external FRP reinforcement reduces the crack spacing to a great extent. This corresponds with the observation made by several researchers[9]. The denser the crack spacing, the smaller the crack width.

ANALYTICAL VERIFICATION

Tension stiffening

The tension stiffening effect was verified by looking to the mean tensile strain of the prism subjected to tension. The load-strain behavior of these prisms is verified according to Eurocode 2 (2004)[10], defining states 1 and 2 as the uncracked and fully cracked state, respectively. The mean tensile strain follows from

$$\varepsilon_m = (1-\zeta)\varepsilon_1 + \zeta\varepsilon_2 \tag{2}$$

with, ξ a distribution or tension stiffening coefficient defined as:

$$\begin{aligned} \zeta &= 0 && N < N_{cr} \\ \zeta &= 1-\beta\left(\frac{N_{cr}}{N}\right)^n && N > N_{cr} \end{aligned} \tag{3}$$

where N is the applied tensile force, β is a coefficient taking into account the bond characteristics of the reinforcement and loading type (1 in case of deformed steel and short-term loading) and N_{cr} is the cracking load. According to EC2 the power n equals 2. For HSC more accuracy is obtained[11] with n equal to 3.

As it is difficult to separate the effects of the internal steel and the external FRP reinforcement, it is assumed for practical reasons that Eqs. (2) and (3) can be applied in the case of a combination of steel and FRP reinforcement. Accordingly, three branches in the load-strain curves are obtained. The first branch corresponds to state 1, in which the concrete is uncracked or $\varepsilon_m = \varepsilon_1$

$$\varepsilon_1 = N/(E_cA_c + E_sA_s + E_fA_f) \tag{4}$$

The second branch starts after cracking of the concrete and continues as long as the internal steel is not yielding. The term ε_m is calculated using Eq. (2) to (4) with

$$\varepsilon_1 = N/(E_sA_s + E_fA_f)\ \varepsilon_2 \leq \varepsilon_y \tag{5}$$

The third branch corresponds to yielding of the internal steel and the additional load increase is provided by the external reinforcement only. In this case the strain in the fully cracked state becomes

$$\varepsilon_2 = (N - A_sf_y)/E_fA_f\varepsilon_2 > \varepsilon_y \tag{6}$$

For the reference prisms, this third branch was assumed as horizontal. In the model, failure is reached at fracture of the FRP reinforcement, this is if ε_2E_f equals the FRP tensile strength.

Although the bond behavior of FRP differs from that of steel, it is still assumed that $\beta = 1$ and $n = 2$ (3 for HSC) can be adopted, as both materials exhibit good bond characteristics. As demonstrated in Fig. 10, this assumption gives a good agreement between experimental and analytical results. In this figure, in addition to the EC2 model (Eq. (2) to (6)), the model given in the CEB-FIP Model Code (1990)[12] is also given.

A fairly accurate prediction is obtained for both models. The Eurocode 2 (EC2) model gives the best results, whereas the Model Code 1990 (MC90) model generally tends to overestimate the decrease of stiffness during crack formation and overestimates the stiffness at higher load levels. Further, it can be observed that the crack formation happens in a smoother way for the strengthened prisms than for the reference prisms, especially in the case of low reinforcement ratios. For the prisms with high strength concrete, the MC90 model significantly overestimates the tension stiffening effect. This is not the case for the EC2 model where a power n equal to 3 instead of 2 was used for the tension stiffening coefficient.

Moment-curvature and moment-deflection behavior

To verify the beam deflections, the load-curvature behavior at midspan was evaluated first. In addition, the tension stiffening approach discussed in the previous section is utilized. Considering states 1 and 2 as the uncracked and the fully cracked state respectively, the mean curvature $1/r$ follows[10] similar to Eq. (2) as

$$1/r = (1-\zeta)1/r_1 + \zeta 1/r_2 \tag{7}$$

with the tension stiffening coefficient

$$\begin{aligned} \zeta &= 0 && M < M_{cr} \\ \zeta &= 1-\beta\left(\frac{M_{cr}}{M}\right)^n && M > M_{cr} \end{aligned} \tag{8}$$

According to theory of elasticity, the curvatures $1/r_1$ and $1/r_2$ follow from

$$1/r_1 = \frac{M}{E_c I_1} \quad 1/r_2 = \frac{M}{E_c I_2} \tag{9}$$

with, I_1 and I_2 the moments of inertia of the uncracked and cracked section, respectively. The moment of inertia depends on the dimensions of the beam cross-section, the depth of the compression zone, the amount of reinforcement and the stiffness of the reinforcement. Applying equilibrium of forces, it appears that the depth of the compression zone depends on the ratio $\varepsilon_o/\varepsilon_c$ (ε_o is the initial strain at the extreme tension fiber before strengthening and ε_c the concrete strain at the extreme compression fiber). As this ratio is not constant, the moment of inertia depends on the acting load level. However, it was verified that the influence of $\varepsilon_o/\varepsilon_c$ on the calculation is limited (e.g. for the beams in this test program, I_2 varied with 0.2 % maximum) so that $\varepsilon_o/\varepsilon_c$ may be assumed 0.

The above equations are valid for strengthened and unstrengthened members. In reality, to account for the moment at which the strengthening is applied, a combination of both should be considered. Accordingly, the curvature in the cracked state is given as:

$$\begin{aligned} 1/r_2 &= \frac{M}{E_c I_{o2}} && M \le M_o \\ 1/r_2 &= \frac{M-M_o}{E_c I_2} + \frac{M_o}{E_c I_{o2}} && M > M_o \end{aligned} \tag{10}$$

where, I_o is the moment of inertia before strengthening. The curvature $1/r_1$ may be calculated in a similar way. However, as $I_{o1} \approx I_1$, Eq. 9 may still be applied.

Furthermore, it is noted that the flexural stiffness $E_c I_2$ becomes difficult to evaluate after the internal steel starts yielding. To allow the calculation of the curvature for moments larger than M_y and to increase the accuracy, in stead of a linear elastic analysis the curvature in the cracked state can also be calculated based on a non-linear analysis

$$1/r_2 = \frac{\varepsilon_c}{x} \tag{11}$$

where, the concrete strain ε_c at the extreme compression fiber and the depth x of the compression zone are obtained following equilibrium of forces and moments.

The moment-curvature behavior of the beams was verified according to the above two methods: linear and non-linear, taking into account the tension stiffening. The calculation of the cracking moment M_{cr} is based[13] on a concrete tensile strength f_{cm}

$$f_{cr} = 0.62\sqrt{f_{cm}} \tag{12}$$

with, f_{cr} and f_{cm} in MPa [replace 0.62 by 7.5 in Eq. 12, using f_{cr} and f_{cm} in psi]. Results of the calculation are given in Fig. 11. Both methods almost match each other (for $M < M_y$) and give reasonably accurate predictions.

The moment-deflection behavior can be predicted by integration of the curvature along the beam length.

Results are shown in Fig. 12. The midspan deflection has been calculated based on the method of virtual work. As an alternative, which is more simple to calculate, the mean deflection can be derived according to the so-called CEB (Comité Euro-International du Béton) bilinear method[14]

$$a = (1 - \zeta_b)a_1 + \zeta_b a_2 \tag{13}$$

with a_1 and a_2 the deflections in respectively the uncracked and the fully cracked state and ζ_b the distribution (tension stiffening) coefficient

$$\begin{aligned} \zeta_b &= 0 && M < M_{cr} \\ \zeta_b &= 1 - \beta\left(\frac{M_{cr}}{M}\right)^{n/2} && M > M_{cr} \end{aligned} \tag{14}$$

Note, that in the bilinear method the tension stiffening approach is directly applied on the deflections in uncracked and fully cracked state obtained by the theory of elasticity, whereas the tension stiffening coefficient is adapted to this approach (power n in Eq. (8) versus power $n/2$ in Eq. (14)). Whereas the bilinear method is simpler, it appears to slightly underestimate the deflection (right part of Fig. 12).

Cracking

Based on the tension stiffening tests, different approaches for the modelling of the crack width have been verified by Matthys[2] and the best predictions are obtained with a model based on MC90,[12] which considers the bond behaviour of both the internal and external reinforcement. The derived model for strengthened tension members is also applicable to strengthened flexural members. Assuming stabilized cracking, the mean crack width is given[2] by:

$$\begin{aligned} w_m &= s_{rm}\varepsilon_{rm,r} \\ &= s_{rm}\zeta\varepsilon_{r2} \end{aligned} \tag{15}$$

with s_{rm} the mean crack spacing, $\varepsilon_{rm,r}$ the mean strain of the reinforcement with respect to the surrounding concrete, ζ the tension stiffening coefficient according to Eq. (8), and ε_{r2} the reinforcement strain in the cracked section. The mean crack spacing for the strengthened members is given[2,12,15] as

$$s_{rm} = \frac{2 f_{ctm} A_{c,eff}}{\tau_{sm} u_s} \frac{E_s A_s}{E_s A_s + \xi_b E_f A_f} \quad with \quad \xi_b = \frac{\tau_{fm} E_s Ø}{\tau_{sm} E_f 4t} \tag{16}$$

where, $\tau_{sm} = 1.8 f_{ctm}$ and $\tau_{fm} = 1.25 f_{ctm}$ are the mean bond stress of the steel[12] and the FRP,[16] u_s is the bond perimeter of the steel, ξ_b a bond parameter and t is the FRP thickness (total thickness for multiple layers).

Results of the analytical verification of the mean crack width are shown in Fig. 13 for some of the specimens. Fairly accurate predictions are obtained. As the models for the calculation of the crack width are intended to be used at service load level, the accuracy at higher load levels is generally less.

SUMMARY AND CONCLUSIONS

In the case of FRP strengthened members, and depending on the amount and stiffness of the additional reinforcement, an improved serviceability behaviour will be obtained due to the following favorable aspects:

- The addition of external reinforcement causes an increase of the moment of inertia of the cracked section.
- After cracking, the tension forces in a cracked section are only balanced by the reinforcement. However, tension forces are transmitted to the surrounding concrete in between adjacent cracks by bond forces. This contributes to the stiffness in the cracked state ('tension stiffening effect'). Both the internal and external reinforcement will contribute to the tension stiffening effect, due to their capability of transferring bond forces.
- As the external reinforcement relieves some of the tensile stresses carried by the internal steel reinforcement, the bar strains and hence the crack widths are reduced for a given load level.
- The external reinforcement is bridging the cracks, causing an external restraining effect which results in

denser crack spacing and smaller crack widths.

Because already small amounts of FRP increase the failure load to a large extent, the efficiency with respect to the SLS is generally less than that with respect to the ultimate limit state (ULS).

The magnitude of the stiffness in the cracked state strongly depends on the equivalent reinforcement ratio, hence on both the amount and stiffness of the reinforcements. The stiffness in the cracked state after yielding of the internal steel mainly depends on the amount and type of external FRP reinforcement.

Considerably smaller crack spacing and crack widths are obtained for the strengthened prisms. Also, the crack formation happens in a smoother way compared to unstrengthened specimens.

The behaviour of the strengthened elements in terms of mean strains, curvatures, deflections, taking into account the tension stiffening effect, can be predicted in an accurate way. Fairly accurate predictions are also obtained with respect to cracking, though further improvement of models for cracking predictions may be needed.

ACKNOWLEDGMENTS

The authors wish to express their gratitude to IWT and FWO for financing this research work, as well as the different companies who provided testing materials.

REFERENCES

1. Matthys, S.; Taerwe, L.; and De Meyer, P., “Effect of Externally Bonded Fibre Reinforced Polymers on the Tension Stiffening Behaviour of Concrete Prisms,” 2nd International RILEM Symposium on Adhesion Between Polymers and Concrete, RILEM Proceedings, V. 9, 1999, pp. 363-373.

2. Matthys, S., *Structural Behaviour and Design of Concrete Members Strengthened with Externally Bonded FRP Reinforcement*, PhD thesis, Ghent University, Gent, Belgium, 2000, 345 pp.

3. Sato, Y., and Vecchio, F.J., “Tension Stiffening and Crack Formation in Reinforced Concrete Members with Fiber-Reinforced Polymer Sheets,” *Journal of Structural Engineering*, V. 129, No. 6, 2003, pp. 717-724.

4. Ferretti, D., and Savoia., M., “Non-Linear Model for R/C Tensile Members Strengthened by FRP-Plates,” *4th International Conference on Fracture Mechanics of Concrete Structures, Engineering Fracture Mechanics*, V. 70, No. 7-8, 2003, pp. 1069-1083.

5. Ceroni, F.; Pecce, M.; and Matthys, S., “Tension Stiffening of Reinforced Concrete Ties Strengthened with Externally Bonded Fiber-Reinforced Polymer Sheets,” *Journal of Composites for Construction*, V. 8, No. 1, 2004, pp. 22-32.

6. Ebead, U.A., and Marzouk. H., “Tension-stiffening Model for FRP-Strengthened RC Concrete Two-Way Slabs,” *Materials and Structures*, V. 38, No. 276, 2005, pp. 193-200.

7. Hashemi, S.H.; Rahgozar, R.; and Maghsoudi, A.A., “Finite Element and Experimental Serviceability Analysis of HSC Beams Strengthened with FRP Sheets,” *American Journal of Applied Sciences*, V. 4, No. 9, 2007, pp. 725-735.

8. Ceroni, F., and Pecce, M., “Design Provisions for Crack Spacing and Width in RC Elements Externally Bonded with FRP,” *Composites Part B: Engineering*, V. 40, No. 1, 2009, pp. 17-28.

9. Taerwe, L., ed., *Non-Metallic (FRP) Reinforcement for Concrete Structures*, Proceedings of the International RILEM Symposium FRPRCS-2, E&FN Spon, London, UK, 1995, 714 pp.

10. EN 1992-1-1, “Eurocode 2: Design of Concrete Structures—Part 1-1: General Rules and Rules for Buildings,” European Committee for Standardization (CEN), Brussels, Belgium, 2004.

11. Lambotte, H., and Taerwe, L., “Deflection and Cracking of High-Strength Concrete Beams and Slabs,” *Proceedings of the Second International Symposium on High-Strength Concrete*, SP-121, W.T. Hester ed., American Concrete Institute, Farmington Hills, MI, 1990, pp. 109-128.

12. MC90, *CEB-FIP Model Code 1990—Design Code*, Thomas Telford for Comité Euro-International du Béton (CEB), Lausanne, Switzerland, 1993, 473 pp.

13. ACI Committee 318, “Building Code Requirements for Structural Concrete (ACI 318-08) and Commentary,” American Concrete Institute, Farmington Hills, MI, 2008, 473 pp.

14. CEB 158-E, “CEB-Manual Cracking and Deformations,” *CEB Bulletin d’Information*, V. 158-E, Comité Euro-International du Béton (CEB), Lausanne, Switzerland, 248 pp.

15. Rostásy, F.S.; Holzenkämpfer, P.; and Hankers, C., “Geklebte Bewehrung für die Verstärkung von Betonbauteilen,” *Betonkalender 1996*, V. II, 1996, pp. 547-576. (in German)

16. Holzenkämpfer, P., *Ingenieurmodelle des Verbunds geklebter Bewehrung für Betonbauteile*, V. 108, PhD thesis, Technical University Braunschweig, Germany, 1994, 214 pp. (in German)

Table 1—Test parameters RC beams strengthened in flexure

Spec.	Type of strengthening	Age at test, days	f_{cm}, MPa (psi)	ρ_s, %	ρ_f, %	Pre-loading, kN (kips)	Load during strengthening, kN (kips)
BF1	Unstrength. (ref.)	56	33.7 (4888)	0.96	—	—	Self weight
BF2	Strengthened(1)	56	36.5 (5294)	0.96	0.14	—	Self weight
BF3	Strengthened(1)	56	34.9 (5062)	0.96	0.14	—	Self weight
BF4	Pre-cracked/strength.(1)	61	30.8 (4467)	0.96	0.14	110 (24.7)	Self weight
BF5	Strength.(1) while loaded	65	37.4 (5424)	0.96	0.14	110 (24.7)	110 (24.7)
BF6	Strength.(1) & anchored(2)	72	35.9 (5207)	0.96	0.14	—	Self weight
BF7	Unstrength. (ref.)	105	38.5 (5584)	0.48	—	—	Self weight
BF8	Strengthened(1)	107	39.4 (5714)	0.48	0.14	—	Self weight
BF9	Strengthened(3)	59	33.7 (4888)	0.48	0.026	—	Self weight

(1) CarboDur 100 mm x 1.2 mm.
(2) Replark 330 mm x 0.111 mm.
(3) 2 layers Replark 100 mm.
Note: 1 mm = 0.03937 in.

Table 2—Mean properties obtained by tensile testing

Type	Nominal dimensions, mm (in.)	Yield strength, MPa (psi)	Tensile strength, MPa (psi)	Ultimate strain, %	E-modulus, GPa (ksi)
Rebar S500	Ø 10 (0.39) Ø 14 (0.55) Ø 16 (0.63)	590 (85570) 550 (79770) 590 (85570)	670 (97175) 630 (91375) 690 (100075)	nm nm 12.4	200 (29010)
CarboDur S1012	100 × 1.2(1) (3.94 × 0.047)	—	3200 (464120)	1.85	159 (23060) (3)
Replark MRK-M2-20	100 × 0.111(2) (3.94 × 0.0044)	—	3500 (507630)	1.25	233 (33795) (3)
Roviglas G	100 × 0.100(2) (3.94 × 0.0044)	—	1300 (188550)	2.07	57 (8265) (3)

(1) Global thickness.
2) Equivalent dry-fiber thickness.
(3) Tangent modulus at the origin.
Note: nm = not measured

Table 3—Test parameters of the tension stiffening tests

Batch	Specimen	Age at test	f_{cm}, MPa (psi)	Steel reinf.	ρ_s, %	FRP type	FRP layers	ρ_f, %	ρ_{eq}, %
T1	N(T1)/100/14/Ref.	28	36.2 (5250)	Ø 14 (0.55)	1.56	—	—	—	—
	N(T1)/100/14/C#1	29		Ø 14 (0.55)	1.56	CFRP	1	0.23	1.82
	N(T1)/100/14/C#2	29		Ø 14 (0.55)	1.56	CFRP	2	0.45	2.08
T2	N(T2)/100/14/C#1	36	32.3 (4685)	Ø 14 (0.55)	1.56	CFRP	1	0.23	1.82
	N(T2)/100/14/G#2	28		Ø 14 (0.55)	1.56	GFRP	2	0.41	1.68
	N(T2)/100/14/G#5	29		Ø 14 (0.55)	1.56	GFRP	5	1.02	1.85
T3	N(T3)/100/10/Ref.	27	32.5 (4714)	Ø 10 (0.39)	0.79	—	—	—	—
	N(T3)/100/10/C#1	28		Ø 10 (0.39)	0.79	CFRP	1	0.22	1.05
	N(T3)/100/10/G#5	28		Ø 10 (0.39)	0.79	GFRP	5	1.01	1.08
	N(T3)/100/10/C#4	29		Ø 10 (0.39)	0.79	CFRP	4	0.90	1.82
T4	N(T4)/100/16/Ref.	28	30.3 (4395)	Ø 16 (0.63)	2.05	—	—	—	—
	N(T4)/100/16/C#1	28		Ø 16 (0.63)	2.05	CFRP	1	0.23	2.31
	N(T4)/100/16/G#5	29		Ø 16 (0.63)	2.05	GFRP	5	1.02	2.34
	N(T4)/100/14/C#3	29		Ø 14 (0.55)	1.56	CFRP	3	0.68	2.34
T5	H(T5)/100/14/Ref.	27	96.0 (13924)	Ø 14 (0.55)	1.56	—	—	—	—
	H(T5)/100/14/C#1	27		Ø 14 (0.55)	1.56	CFRP	1	0.23	1.82
	H(T5)/100/14/G#2	28		Ø 14 (0.55)	1.56	GFRP	2	0.41	1.68
	H(T5)/100/14/G#3	28		Ø 14 (0.55)	1.56	GFRP	3	0.61	1.74

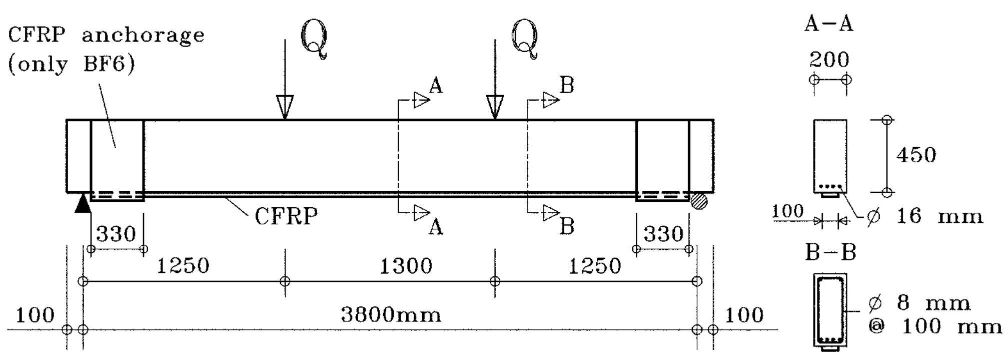

Fig. 1—Test setup and specimen dimensions. (Note: 1 mm = 0.03937 in.)

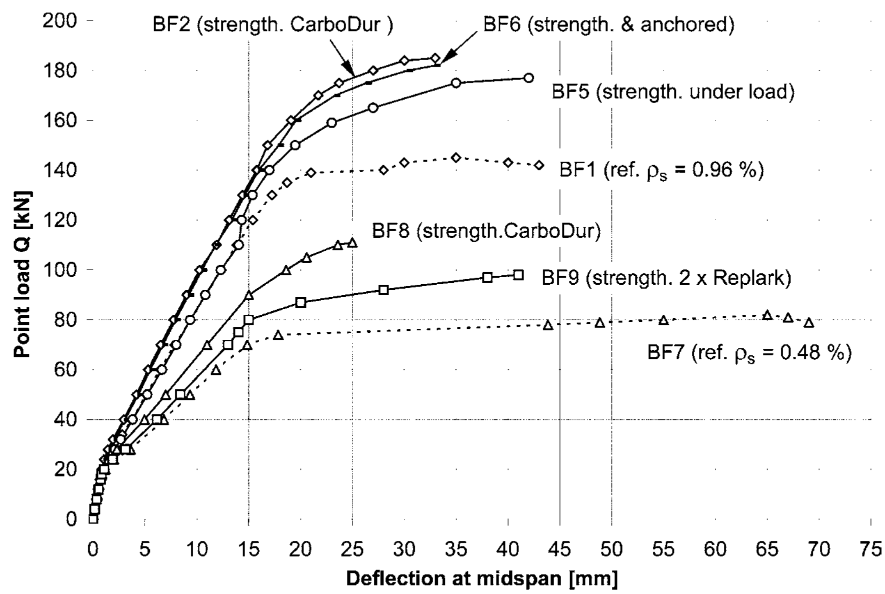

Fig. 2—Load-deflection behavior of Beams BF1,2,5,6,7-9. (Note: 1 kN = 0.2248 kips; 1 mm = 0.03937 in.)

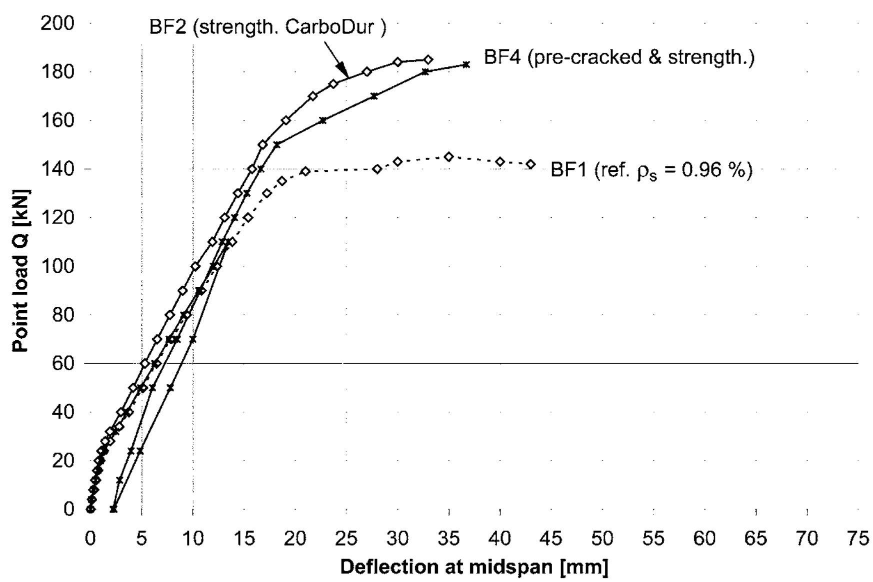

Fig. 3—Load-deflection behavior of Beams BF1,2,4. (Note: 1 kN = 0.2248 kips; 1 mm = 0.03937 in.)